



HAL
open science

Electromigration of Au on Ge(111): Adatom and island dynamics

F. Leroy, A. El Barraï, F. Cheynis, P. Müller, S. Curiotto

► **To cite this version:**

F. Leroy, A. El Barraï, F. Cheynis, P. Müller, S. Curiotto. Electromigration of Au on Ge(111): Adatom and island dynamics. *Physical Review B*, 2022, 106 (11), pp.115402. 10.1103/PhysRevB.106.115402 . hal-03778391

HAL Id: hal-03778391

<https://hal.science/hal-03778391v1>

Submitted on 15 Sep 2022

HAL is a multi-disciplinary open access archive for the deposit and dissemination of scientific research documents, whether they are published or not. The documents may come from teaching and research institutions in France or abroad, or from public or private research centers.

L'archive ouverte pluridisciplinaire **HAL**, est destinée au dépôt et à la diffusion de documents scientifiques de niveau recherche, publiés ou non, émanant des établissements d'enseignement et de recherche français ou étrangers, des laboratoires publics ou privés.

Electromigration of Au on Ge(111): *adatom* and island dynamics

F. Leroy,^{1,*} A. El Barraï,¹ F. Cheynis,¹ P. Müller,¹ and S. Curiotto¹

¹*Aix Marseille Univ, CNRS, CINAM, AMU-TECH, Marseille, France*

(Dated: August 22, 2022)

We have observed the motion of two-dimensional phases of Au on Ge(111) under an electric bias by *in operando* low energy electron microscopy. Electromigration of Au results in a complex dynamics that depends on the nature of the involved mobile phases: two-dimensional *adatom* gas or two-dimensional islands. We show that the Au *adatoms* move at the surface in the direction opposite to the electric current. The wind force induced by the electron flow is measured: the effective valence of Au ($Z^* = -82 \pm 15$) is directly deduced from the coverage profile of a Au *adatom* gas spatially retained by a strong Ehrlich-Schwoebel barrier at a down-hill step edge. The velocity of two-dimensional Au islands versus island size reveals a mass transport by terrace diffusion inside the islands. The energy barrier for diffusion above 820 K is 1.16 ± 0.08 eV and it strongly increases up to 3.1 ± 0.6 eV below. We attribute this change of regime to a modification of diffusing species from single Au atoms at high temperature to Au clusters at low temperature. The strong shape fluctuations of the 2D-islands is consistent with a nearly vanishing line tension of 1.2 ± 0.4 meV/nm at 800 K.

Mass transport phenomena occurring at solid surfaces are crucial in the context of nanofabrication and growth processes. To study these phenomena one approach consists in analyzing the fluctuation dynamics of surface structures such as island edges [2–4] or their response to a perturbation [5]. In that respect mass transport induced by an electric current [6–8] provides a unique opportunity to study atomic processes using the electric current as a perturbation of the random processes occurring at the surface [9–12]. For instance the size-dependence of the velocity of 2D-islands that are displaced by a flowing electric current is intimately related to the atomic processes of diffusion and attachment-detachment at step edges [13–15]. If there is a key benefit of studying a directed motion rather than a random motion from a statistical analysis point of view, the counterpart is to know quantitatively the applied force. Historically electromigration has been studied in solids and thin films [7, 8, 16–18]. It has been proposed that the driving force for atom migration arises from two sources: (i) the external electric field acts directly on the partially charged atoms and the driving force is called direct force, (ii) the electric current carriers transfer a momentum to the atoms, this results in a driving force called the wind force [19–21]. The experimental determination of the dominant force and the quantification of the effective *adatom* valence are still very rare [9] and call for dedicated studies [7 and 8]. In addition electromigration phenomena of *adatoms* at surfaces [7, 8, 18–23] can cause substantial changes in the surface morphology such as step bunching for vicinal surfaces [16, 17, 24, and 25] or shape instabilities of 2D islands [5, 10, 26–28]. These surface modifications are also intimately related to the dominant mass transport phenomenon.

This article aims at addressing the mechanisms of Au transport on Ge(111), *i.e.* the diffusivity of Au, the energy barriers involved in mass transport, as well as the effective valence of the *adatoms*. In that purpose, and to disentangle the different terms that are involved in the

electromigration process, the results rely on the analysis of the migration phenomena of two-dimensional (2D) layers of Au in different states: gas, Au-rich and Au-poor 2D islands. This study is based on an *in operando* observation under an electric current of the Au-Ge(111) surface by low energy electron microscopy (LEEM). The experimental set-up allows to study the spatio-temporal dynamics at a surface [29 and 30]. At high temperature (above ~ 800 K) using the 2D *adatom* gas coverage profile nearby a step edge we determine the effective valence of Au *adatoms* at the Ge(111) surface responsible for the wind force ($Z^* = -82 \pm 20$). Decreasing the temperature the gas phase condenses into a 2D dilute phase of Au (Au-poor phase) and forms 2D islands on Ge(111). The electromigration velocity of these islands versus the island size claims for a mass transport phenomenon limited by terrace diffusion inside the islands. In addition the large fluctuations of the island edges indicate a vanishingly small line tension of 1.2 ± 0.4 meV/nm at 800 K. At even lower temperature (or higher Au coverage) a dense Au-rich phase forms that is comparatively immobile. The apparent migration of this phase is induced by phase transformation with the surrounding Au-poor phase and is limited by mass transport kinetics *via* terrace diffusion mechanism inside the Au-poor phase. We demonstrate the possible generation of Au-rich or Au-poor 2D-islands.

I. EXPERIMENTAL

Ge(111) wafers are first cut ($0.5 \times 4 \times 17$ mm³) and cleaned by acetone and ethanol rinsing before introduction in ultra-high vacuum (UHV, 10^{-8} Pa). Then they are cleaned by repeated cycles of ion bombardment (Ar⁺, $E=1$ keV, $I=8$ μ A) and annealing (1000 K). At last, the crystals are annealed close to the Ge melting point (1211 K) during a few seconds to obtain extended (111) terraces at the surface [15] (>10 μ m²). The electric cur-

rent is applied in the $\langle 110 \rangle$ direction. The sample temperature is adjusted independently from the electric current by using a complementary radiative W filament and an electron bombardment heating stage [32]. The temperature is measured with an Impac pyrometer ($\epsilon=0.56$) that has been calibrated using the Ge(111)-($\sqrt{3} \times \sqrt{3}$)-Au to $-(1 \times 1)$ -Au surface phase transition occurring at 913 K for 1 monolayer (ML) [4] and the eutectic melting point of Au-Ge droplets (634 K). The absolute temperature precision is about 50 K in the range 600 - 900 K. Au is deposited by evaporation-condensation using a MBE-Komponenten GmbH effusion cell containing 5N Au shots. We deposit less than 1 ML of Au on Ge(111) to avoid the formation of Au-Ge droplets. Since the solubility of Au into Ge bulk crystal is less than 10^{-4} at. % at the solid state, Au dissolution is negligible [31]. The migration of Au is studied by low energy electron microscopy (LEEM III, Elmitec GmbH) in bright field mode, with an electron-beam energy of 6.0 eV. Low energy electron diffraction (LEED) patterns are measured at various electron energies in the range 3-30 eV.

II. RESULTS AND DISCUSSION

A. 2D-gas phase of Au on Ge(111): the determination of the Au adatom valence

LEEM image in figure 1(a) shows the surface of a Ge(111) single crystal at 830 K covered with about 0.25 ML of Au under an applied electric current ($j=1.2 \cdot 10^6$ A.m $^{-2}$). This surface is obtained after a sharp temperature drop from 900 K. Initially the surface looks homogeneous, *i.e.* covered with a uniform gas of Au adatoms. After a temporary evolution of less than a minute, the surface reaches a stationary state with smooth intensity variations and no border as expected for a gas phase. The intensity contrast at the surface varies in the direction of the electric current (see supplementary movie S1 [33]). It is clear that the down-hill step edge of the substrate, perpendicular to the electric current, acts as a Erlich-Schwobel barrier [4, 34, and 35] such that the Au adatoms cannot cross them easily. Assuming that the intensity contrast is linearly related to the local coverage of the Au adatom gas [30] we can extract the coverage profile of the Au adatoms at the surface (see fig. 1-(b)). Theoretically we can calculate the stationary coverage profile of the adatom gas from Maxwell-Boltzmann statistics considering an external force on adatoms and an impermeable boundary at the down-hill step edge (assuming also that the adatoms do not interact with each other). This coverage profile results from the balance between the flux of adatoms due to the electromigration force and the opposite flux arising from the coverage gradient (Fick's law). The flux of adatoms due to the electromigration force reads $j_{el} = \frac{Dc_{Au}}{k_B T} F$ where D is the Au diffusion coefficient, c_{Au} is the local Au adatom coverage, k_B is the Boltzmann constant, T is the temperature

and $F = eZ^*E$ is the electromigration force (E is the applied electric field and e is the elementary charge). The flux arising from the coverage gradient is $j_c = -D \frac{\partial c_{Au}}{\partial x}$. Theoretically the Au adatom gas coverage profile reads:

$$c_{Au} = c_{Au,s} e^{-\frac{\epsilon_p}{k_B T}} \quad (1)$$

where $c_{Au,s}$ is the maximum Au coverage close to the step edge and $\epsilon_p = -eZ^*E \cdot x$ is the potential energy of Au adatoms under an electric bias. This potential energy is proportional to the distance x with respect to the maximum of coverage (close to the step). From the experimental profile $c(x) = c_{Au,s} e^{\frac{x}{\xi}}$ we can estimate the electromigration length $\xi = \frac{k_B T}{eZ^*E} = -5500 \pm 1000$ nm (see experimental fit in fig. 1-(b)) and therefore the valence of Au adatoms $Z^* = -82 \pm 15$ ($E = 150$ V/m). The sign of Z^* shows that the Au adatoms displace in the direction of the electron flow. This value is within the range of calculated values for metal adatoms [36–39] and is consistent with a dominant wind force. The calculated force is $F = eZ^*E = -1.2 \pm 0.2 \cdot 10^{-5}$ eV/nm = $-2.0 \pm 0.4 \cdot 10^{-15}$ N. It acts as a weak perturbation with respect to the random thermal diffusion process ($\frac{F a}{k_B T} \ll 1$ where a is an atomic distance). Contrary to previous estimates of the valence of atoms that involve mass transfer measurements [40 and 41] and therefore a prior evaluation of the diffusivity of the entities Dc and/or surface instability modeling [42–45], here it is remarkable that this result involves a straightforward modeling and no free parameter except Z^* .

B. 2D Au-poor phase on Ge(111)

When the temperature is below 800 K and for low Au coverage (below 0.367 ML [4]), the Au adatom gas condenses into 2D-islands that electromigrate in the direction of the electron flow (see fig. 2-(a)-(c)). The LEED patterns show a Ge(111)-(1×1)-Au surface reconstruction for the islands and a diffuse Ge(111)-(2×1) reconstruction for the surrounding surface (see fig. 2(b)). This latter surface structure occurs on Ge(111) in presence of remaining Au adatoms at the surface that disorganize the $c(2 \times 8)$ reconstruction of the pure Ge(111) surface [46 and 47]. The Ge(111)-(2×1) reconstruction transforms into a splitted Ge(111)-(2×2) structure [48] at RT and shows a similar LEED pattern as the Ga-induced Ge(111) surface reconstruction [49] (see fig. 2-(b)). Concerning the Ge(111)-(1×1)-Au phase of the islands formed by condensation of the Au adatom gas, it evolves into the Ge(111)-($\sqrt{3} \times \sqrt{3}$)-Au reconstruction at RT [4]. This phase change is accompanied by a strong area shrinking of the islands by a factor ~ 3 (see fig. 2-(c)). As deduced by Giacomo and coworkers [4], the Au coverage inside the Ge(111)-(1×1)-Au phase is about 0.367 ML (the Ge(111)-($\sqrt{3} \times \sqrt{3}$)-Au phase has a Au coverage of 1 ML [50]). We denote in the following the Ge(111)-(1×1)-

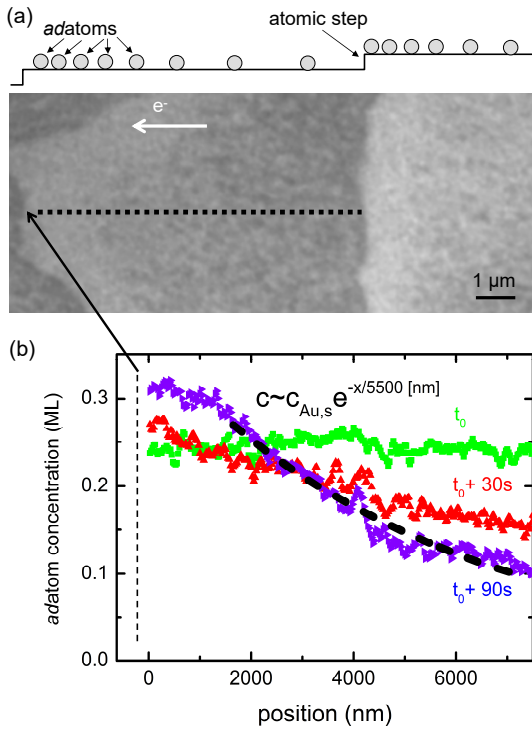


FIG. 1. (a) LEEM image (bright-field mode) of Au (~ 0.25 ML) on Ge(111) at 830 K. The black arrows show atomic steps. (b) coverage profile of Au *adatoms* extracted from the intensity (corrected from inhomogeneous illumination) along the dashed line of (a). The dashed line corresponds to the best fit of the Au adatom coverage profile using $c(x) = c_{Au,s} e^{-x/\xi}$ (see text). $\xi = -5500 \pm 1000$ nm gives the best agreement.

$$v = \frac{Dc}{k_B T} F = \frac{Dc_{Au}}{\xi} \quad (2)$$

209 Considering a mean island velocity of 26 nm/s (see
210 fig. 2-(c)) we can estimate the Au diffusivity on Ge(111)
211 $D_{c_{Au}} = 1.4 \pm 0.4 \cdot 10^5 \text{ nm}^2 \text{ s}^{-1}$ assuming that the effective
212 valence of Au is preserved ($Z^* = -82$).

213 Furthermore, we observe that the 2D islands exhibit
214 very large shape fluctuations (see fig. 2-(a), 3-(a) and
215 supplementary movie S2 [51]). While the area of the is-
216 lands is approximately fixed, the perimeter exhibits large
217 variations over time [see fig. 3-(b)]. The normalized
218 standard deviation of the perimeter is 15 ± 2 %. In addi-
219 tion the mean shape is far from being circular: the ratio
220 of the effective island radius deduced from the perime-
221 ter ($r_P = \frac{P}{2\pi}$) and the radius deduced from the area
222 ($r_A = \sqrt{\frac{A}{\pi}}$) is about 2 indicating a strongly non-circular
223 shape (one for a disk). The large shape fluctuations may
224 explain the slight increase of the islands velocity with the
225 island size (see fig. 2-(c)).

226 To quantify these fluctuations and estimate the line
227 tension stiffness $\tilde{\beta}$ that tends to keep the shape com-
228 pact, we have analyzed the auto-correlation function of
229 a straight edge of a Ge(111)-(1×1)-Au domain pushed
230 onto a Ge step (the electric current is perpendicular to
231 the island, see Fig. 3-(c)). Since mass transport is domi-
232 nated by terrace diffusion as deduced from previous size-
233 dependent velocity measurements, the auto-correlation
234 function $G(t) = \langle [x(y, t) - x(y, 0)]^2 \rangle$ of the step edge po-
235 sition is theoretically given by [52]:

$$G(t) = 0.86 \left(\frac{\Omega k_B T}{\tilde{\beta}} \right)^{2/3} (2Dc \times t)^{1/3} \quad (3)$$

185 Au (resp. Ge(111)-($\sqrt{3} \times \sqrt{3}$)-Au) surface reconstruction
186 as the Au-poor phase (resp. Au-rich phase).

187 To determine the mass transport phenomena respon-
188 sible for the directed migration of the 2D Au-poor is-
189 lands, size-dependent island velocity measurements have
190 been performed (see fig. 2-(d)). The islands drift ve-
191 locity is rather size-independent (only a weak velocity
192 increase is measured). Pierre-Louis *et al.* [5] have the-
193 oretically studied the islands velocity under electromi-
194 gration in the framework of the linear response theory.
195 The velocity v shows different scaling laws with respect
196 to the island size (r) for different mass transport phe-
197 nomena: periphery diffusion ($v \sim r^{-1}$), terrace diffusion
198 (v is size-independent) or attachment-detachment at step
199 edges ($v \sim r$). From the fit of the experimental data with
200 the different mass transport phenomena, the dominating
201 one is more likely to be terrace diffusion. Furthermore,
202 since the islands migrate in the same direction as the Au
203 atoms (electron flow), we deduce that the terrace diffu-
204 sion mechanism occurs within the islands and not from
205 the surrounding surface. This result is in agreement with
206 the low surface density of Au atoms in the Au-poor is-
207 lands [4] that allows numerous diffusion paths for atoms.
208 Within this framework the 2D-islands velocity reads [5]:

236 where $\Omega = 0.139 \text{ nm}^2$ is the atomic area. From the
237 fit of the experimental auto-correlation function $G(t) =$
238 $(810 \pm 250) \times t^{0.33}$ we derive $\tilde{\beta} = 1.2 \pm 0.4 \text{ meV/nm}$ (see
239 fig. 3-(d)). As expected from the large shape fluctu-
240 ations, this line tension is vanishingly small, *e.g.* two
241 orders of magnitude lower than usual step line tensions
242 at the surface of semiconductors (*e.g.* 600 meV/nm for
243 Si(111) step at $\sim 1100 \text{ K}$ [2]) or metals (*e.g.* 300-400
244 meV/nm for Pt(111) step at $\sim 500 \text{ K}$ [52]). It is also
245 consistent with the proximity to the transition tempera-
246 ture of the 2D islands into a 2D Au *adatom* gas at the Ge
247 surface. Such large fluctuations have also been observed
248 in the context of Pb 2D-layers on Ge(111) that fluctuate
249 between two surface phases of similar atomic density [3
250 and 4]. However in this case we infer that the fluctuations
251 arise from an extremely small line tension related to the
252 low atomic density of the Ge(111)-(1×1)-Au 2D phase
253 ($c_{Au} \sim 0.367 \text{ ML}$, [4]) that makes the atomic interactions
254 weak.

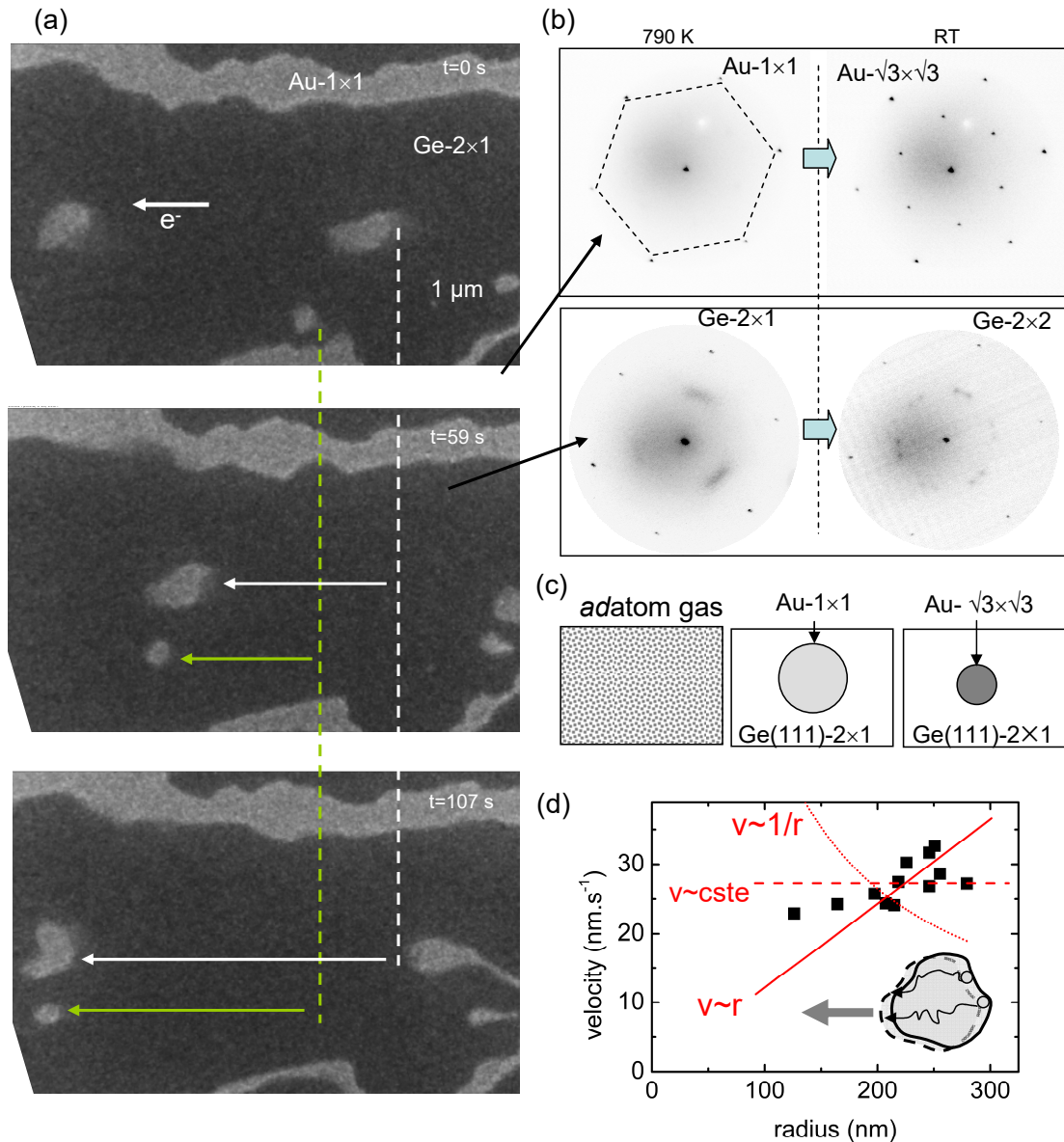


FIG. 2. (a) Series of three LEEM images (bright-field mode) of Ge(111)-(1 × 1)-Au islands electromigrating on Ge(111) at ~790 K. Ge(111)-(1 × 1)-Au islands have a bright contrast whereas the remaining surface (Ge(111)-(2 × 1)) is darker. The white and green arrows show the displacement of the islands over time. The white arrow indicates the direction of the electron flow. (b) LEED pattern (E=14 eV) of the Ge(111)-(1 × 1)-Au reconstructed islands at 790 K and phase transition into the Ge(111)-(√3 × √3)-Au at RT. LEED pattern of the Ge(111)-(2 × 1) at 790 K (average projection of 80 LEED patterns between 3 and 14 eV) and phase transition into the splitted reconstruction Ge(111)-(2 × 2) at RT (LEED at E=14 eV). (c) Schematics of the phase transformation from 2D-gas, Au-poor Ge(111)-(1 × 1)-Au island and Au-rich Ge(111)-(√3 × √3)-Au phase. (d) Size-dependence of the velocity of the Ge(111)-(1 × 1)-Au. The radius is obtained as $\sqrt{A/\pi}$ where A is the island area. Best fit considering different mass transport mechanisms: terrace diffusion (dashed line), periphery diffusion (dotted line) and attachment-detachment (red line). Inset: schematic of the principle of mass transport by terrace diffusion inside the island.

255 C. 2D Au-islands electromigration on Ge(111)

256 Upon cooling at about 770 K, the Au-poor islands
 257 shrink into Au-rich islands, *i.e.* Ge(111)-(√3 × √3)-Au
 258 islands. The Au-rich islands do not move on the Ge(111)-
 259 (2 × 1) surface under the electric bias (velocity detection

260 limit is about 1 nm/s). As it is a Au-rich phase, with a
 261 nominal Au coverage of 1 ML, it does not permit inner
 262 mass transport by terrace diffusion, except *via* vacancies.
 263 This reduces drastically the Au-rich islands velocity as
 264 compared to the velocity of the Au-poor islands. How-
 265 ever, at larger Au coverage ($0.367 \text{ ML} < c_{Au} < 1 \text{ ML}$),
 266 the Au-rich and Au-poor phases coexist at the surface

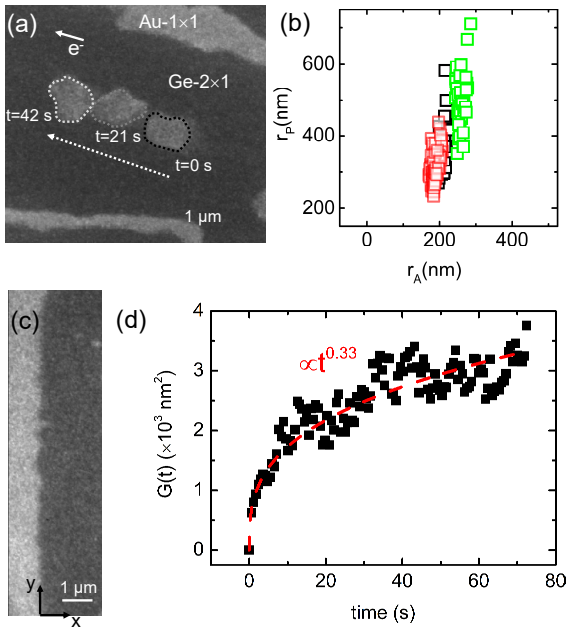


FIG. 3. (a) Projection of three LEEM images measured at $t=0$, 21 and 42 s. The shape changes are illustrated by dotted contour lines. (b) Plot of the effective island radius r_P deduced from the perimeter versus the effective radius r_A deduced from the island area and considering a circular shape (each color correspond to an electromigrating island upon ~ 50 time steps). While the area is approximately constant, the perimeter shows large variations. (c) LEEM image of an extended Ge(111)-(1 \times 1)-Au domain compressed onto a surface step. (d) Time-dependence of the autocorrelation function $G(t)$ of the free edge of the domain and fit assuming $G(t) \sim t^{1/3}$.

and in this case, figure 4(a) shows Au-poor islands electromigrating inside the Au-rich phase (see movie in supplementary materials S3 [53]). The Au-poor islands are generated regularly at the edge of a large terrace and this process is phenomenologically similar to the generation of bubbles in fluids. The reverse situation also occurs [see figure 4(b)]. Size-dependent measurements of the islands velocity show that it is strictly independent of the size [see figure 4(d)]. In addition the Au-poor and Au-rich phases electromigrate both in the same direction, *i.e.* opposite to the electron flow. This clearly evidence that the Au atoms are moving by terrace diffusion (size-independent velocity argument) inside the Au-poor phase [same direction argument; see models in insets of figures 4(a,b)]. To explain the apparent motion of the Au-rich phase whereas diffusion is strongly hindered inside we have to invoke an interfacial mechanism of phase transformation at the interface between the Au-rich and Au-poor phases. Considering the electromigration of Au-poor islands, the Au-rich phase transforms into the Au-poor phase at the front of the island and vice versa at the back. This phenomenon is kinetically equivalent to an attachment-detachment process. Therefore

we can infer that the electromigration of these islands results from a two-step process: (i) terrace diffusion of Au to reach the interface between the two phases and (ii) phase transformation. The size-dependent island velocity measurements indicate that the kinetics of phase transformation is much faster than the time scale for atoms to cross the island by terrace diffusion. Interestingly we can also see that the island shape do not show significant fluctuations. This observation can be related to a large atomic density of the Au-rich phase that imposes a large line tension stiffness at the boundary with the Au-poor phase. Let us note that the absence of shape fluctuations and the size-independence of the islands velocity reinforce our proposal that the small size-dependence of the velocity of the Au-poor islands on the Ge(111)-2 \times 1 surface is related to the shape fluctuations. To estimate the activation energy E_a involved in the Au diffusivity ($Dc_{Au} = D_0c_0e^{-\frac{E_a}{k_B T}}$) of the migrating islands (D_0c_0 is a constant prefactor), we have performed islands velocity measurements in the temperature range 800-900 K [see figure 4-(c)]. The islands reach a maximum velocity of about 850 nm/s at 900 K. The Arrhenius plot of $\frac{vk_B T}{\Omega e E} = Z^* Dc_{Au}$ shows two slopes: above 820 K, the activation energy of Au on Ge(111)-(1 \times 1)-Au surface is $E_a = 1.16 \pm 0.08$ eV and below 820 K the activation energy strongly increases and reaches $E_a = 3.1 \pm 0.6$ eV. Whereas the small activation energy above 820 K is compatible with atomic diffusion, the large energy barrier below 820 K should involve the surface diffusion of complex species such as small clusters. Nakatsuji and coworkers [54] have shown by scanning tunneling microscopy (STM) that there are two typical structures randomly distributed on the Ge(111)-($\sqrt{3} \times \sqrt{3}$)-Au surface: triangle structures and clusters and their density depend strongly on the surface coverage of the Ge(111)-($\sqrt{3} \times \sqrt{3}$)-Au phase and on temperature. Although these experiments were performed at lower temperature, they provide an indication for interpreting the large increase of the activation energy of Au mass transport below 820 K by considering large size mobile entities such as Au clusters.

III. CONCLUSION

In conclusion we have studied the electromigration of 2D Au-layers on Ge(111) in the range 750 K - 900 K. Depending on the coverage and temperature we have put in evidence the presence of a 2D atomic gas, a Au-poor 2D-phase (Ge(111)-(1 \times 1)-Au), and a Au-rich 2D-phase (Ge(111)-($\sqrt{3} \times \sqrt{3}$)-Au). The stationary coverage profile of the Au adatom gas phase provides a quantitative estimate of the effective valence of Au atoms ($Z^* = 82 \pm 15$) involved in the electromigration wind force assuming a perfect gas and a strong Ehrlich-Schwoebel barrier at the step edge. At lower temperature and/or higher Au coverage, the Ge(111)-(1 \times 1)-Au phase occurs forming 2D islands that electromigrate in the direction of the electron flow. The weak size-dependence of the islands

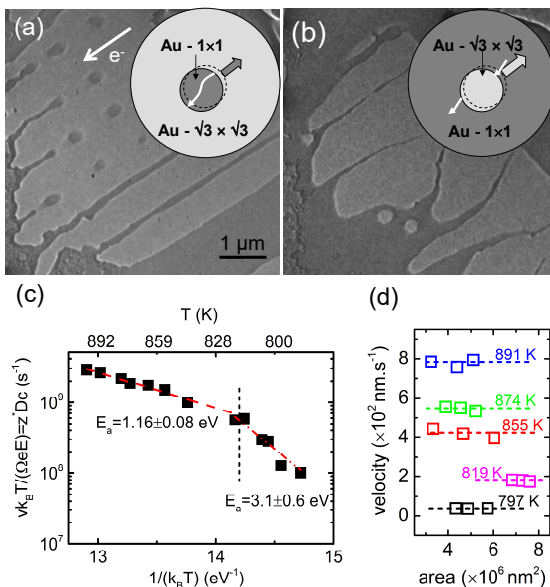


FIG. 4. (a) LEEM image (bright-field mode) of electromigrating Ge(111)-(1x1)-Au islands in Ge(111)-(sqrt(3) x sqrt(3)) phase (scale bar 5 micrometers). (b) LEEM image (bright-field mode) of electromigrating Ge(111)-(sqrt(3) x sqrt(3))-Au islands in Ge(111)-(1x1)-Au phase at 830 K. Insets of (a) and (b): model of mass transfers. (c) Arrhenius plot of the 2D islands $\frac{v_{k_e T}}{\Omega Z^* e E}$. (d) Velocity of islands as function of island size and for different temperatures. At a given temperature, the island velocity is size-independent (dashed guide line).

345 velocity claims for a dominant terrace diffusion mecha-
 346 nism of mass transport inside the islands. By address-
 347 ing the position fluctuations of a straight edge of the
 348 Ge(111)-(1x1)-Au phase we quantitatively estimate the
 349 line tension stiffness. It is vanishingly small due to the
 350 weak atomic interactions that perfectly match the low
 351 surface density of atoms in this phase. The Increase
 352 of the Au coverage allows the coexistence of the dilute
 353 Ge(111)-(1x1)-Au phase (Au-poor) and a dense Ge(111)-
 354 (sqrt(3) x sqrt(3))-Au phase (Au-rich). We were able to obtain
 355 Au-poor 2D-islands migrating into the Au-rich phase and
 356 vice-versa. The 2D-islands electromigrate *via* diffusion
 357 inside the Au-poor phase and phase transformation at
 358 the interface with the Au-rich phase. We have shown
 359 by size-dependent measurements of the islands velocity
 360 that the limiting mass transport mechanism is terrace
 361 diffusion and the interfacial phase transformation phe-
 362 nomenon does not limit the kinetics of mass transfers.
 363 From the Arrhenius plot of the velocity we demonstrate
 364 the presence of two regimes: above 820 K, the activa-
 365 tion energy involved in the Au diffusivity is 1.16 ± 0.08
 366 eV whereas it increases steeply below and reach 3.1 ± 0.6
 367 eV. We attribute this change of behavior to a change of
 368 diffusing species from Au atoms to small Au clusters re-
 369 spectively at high and low temperature.

370 This work has also been supported by the ANR grants
 371 HOLOLEEM (ANR-15-CE09-0012). We thanks Olivier
 372 Pierre-Louis (ILM, Lyon, France) for the fruitful discus-
 373 sions on mass transport processes at surfaces.

374 * frederic.leroy.3@univ-amu.fr

375 ¹ A. S. Frolov, J. Sanchez-Barriga, C. Callaert, J. Hader-
 376 mann, V. A. Fedorov, D. Y. Usachov, A. N. Chaika,
 377 B. C. Walls, K. Zhussupbekov, V. I. Shvets, M. Muntwiler,
 378 M. Amati, L. Gregoratti, A. Y. Varykhalov, O. Rader, and
 379 V. L. Yashina, Atomic and Electronic Structure of a Mul-
 380 tidomain GeTe Crystal, ACS Nano 14, 16576 (2020).
 381 ² A. B. Pang, K. L. Man, M. S. Altman, T. J. Stasevich,
 382 F. Szalma, and T. L. Einstein, Step line tension and step
 383 morphological evolution on the Si(111) (1x1) surface Phys.
 384 Rev. B 77, 115424 (2008).
 385 ³ Y. Sato, S. Chiang, and N. C. Bartelt, Spontaneous do-
 386 main switching during phase separation of Pb on Ge(111)
 387 Phys. Rev. Lett. 99, 096103 (2007).
 388 ⁴ J. A. Giacomo, C. H. Mullet, and S. Chiang, Growth,
 389 phase transition, and island motion of Au on Ge(111) J.
 390 Chem. Phys. 155, 054701 (2021).
 391 ⁵ O. Pierre-Louis and T. L. Einstein, Electromigration of
 392 single-layer clusters Phys. Rev. B 62, 13697 (2000).
 393 ⁶ I. A. Blech and E. S. Meieran, Electromigration in Thin
 394 Al Films J. Appl. Phys. 40, 485 (1969).
 395 ⁷ P. S. Ho and T. Kwok, Electromigration in metals Rep.
 396 Prog. Phys. 52, 301 (1989).
 397 ⁸ H. Yasunaga and A. Natori, Electromigration on semicon-
 398 ductor surfaces Surf. Sci. Rep. 15, 205 (1992).
 399 ⁹ C. Tao, W. G. Cullen, and E. D. Williams, Visualizing the
 400 Electron Scattering Force in Nanostructures Science 328,

401 736 (2010).

402 ¹⁰ A. Kumar, D. Dasgupta, C. Dimitrakopoulos, and
 403 D. Maroudas, Current-driven nanowire formation on sur-
 404 faces of crystalline conducting substrates Appl. Phys. Lett.
 405 108, 193109 (2016).
 406 ¹¹ A. Kumar, D. Dasgupta, and D. Maroudas, Surface
 407 nanopattern formation due to current-induced homoepi-
 408 taxial nanowire edge instability Appl. Phys. Lett. 109,
 409 113106 (2016).
 410 ¹² Q. Liu, R. Zou, J. Wu, K. Xu, A. Lu, Y. Bando, D. Gol-
 411 berg, and J. Hu, Molten Au/Ge Alloy Migration in Ge
 412 Nanowires Nano Lett. 15, 2809 (2015).
 413 ¹³ S. Curiotto, F. Leroy, F. Cheynis, and P. Müller, Self-
 414 propelled motion of Au-Si droplets on Si(111) mediated by
 415 monoatomic step dissolution Surf. Sci. 632, 1 (2015).
 416 ¹⁴ S. Curiotto, F. Leroy, F. Cheynis, and P. Müller, In-Plane
 417 Si Nanowire Growth Mechanism in Absence of External Si
 418 Flux Nano Lett. 15, 4788 (2015).
 419 ¹⁵ S. Curiotto, F. Leroy, F. Cheynis, and P. Müller, Surface-
 420 dependent scenarios for dissolution-driven motion of grow-
 421 ing droplets Sci. Rep. 7, 902 (2017).
 422 ¹⁶ F. Leroy, P. Müller, J. J. Metois, and O. Pierre-Louis, Vic-
 423 inal silicon surfaces: From step density wave to faceting
 424 Phys. Rev. B 76, 045402 (2007).
 425 ¹⁷ F. Leroy, D. Karashanova, M. Dufay, J. M. Debierre,
 426 T. Frisch, J. J. Metois and P. Müller Step bunching to
 427 step-meandering transition induced by electromigration on

- 428 Si(111) vicinal surface Surf. Sci. 603, 507 (2009).
429 ¹⁸ Stefano Curiotto, Pierre Müller, Ali El-Barraj, Fabien
430 Cheynis, Olivier Pierre-Louis, and Frederic Leroy, 2D
431 nanostructure motion on anisotropic surfaces controlled by
432 electromigration Appl. Surf. Sci. 469, 463 (2019).
433 ¹⁹ H. B. Huntington and A. R. Grone, Current-induced
434 marker motion in gold wires J. Phys. Chem. Solids 20,
435 76 (1961).
436 ²⁰ I. A. Blech, Electromigration in thin aluminum films on
437 titanium nitride J. Appl. Phys. 47, 1203 (1976).
438 ²¹ A. H. Verbruggen, Fundamental questions in the theory of
439 electromigration IBM J. Res. Dev. 32, 93 (1988).
440 ²² Stefano Curiotto, Fabien Cheynis, Pierre Muller, and Frederic
441 Leroy, 2D Manipulation of Nanoobjects by Perpendicular
442 Electric Fields: Implications for Nanofabrication ACS
443 Appl. Nano Mater. 3, 1118 (2020).
444 ²³ F. Leroy, A. El Barraj, F. Cheynis, P. Muller, and S. Curiotto,
445 Electric forces on a confined advacancy island Phys.
446 Rev. B 102, 235412 (2020).
447 ²⁴ AV Latyshev, AL Aseev, AB Krasilnikov, and SI Stenin,
448 Transformation on clean Si(111) stepped surface during
449 sublimation Surf. Sci. 213, 157 (1989).
450 ²⁵ Y Homma, RJ MC Clelland, and H Hibino, DC-resistive-
451 heating-induced step bunching on vicinal Si(111) Jpn. J.
452 Appl. Phys. 29, L2254 (1990).
453 ²⁶ P Kuhn, J Krug, F Hausser, and A Voigt, Complex
454 shape evolution of electromigration-driven single-layer
455 islands Phys. Rev. Lett. 94, 166105 (2005).
456 ²⁷ Ashish Kumar, Dwaipayana Dasgupta, and Dimitrios
457 Maroudas, Complex Pattern Formation from Current-
458 Driven Dynamics of Single-Layer Homoepitaxial Islands
459 on Crystalline Conducting Substrates Phys. Rev. Appl.
460 8, 014035 (2017).
461 ²⁸ Stefano Curiotto, Frederic Leroy, Pierre Muller, Fabien
462 Cheynis, Michail Michailov, Ali El-Barraj, and Bogdan
463 Ranguelov, Shape changes of two-dimensional atomic
464 islands and vacancy clusters diffusing on epitaxial (111)
465 interfaces under the impact of an external force J. Cryst.
466 Growth 520, 42 (2019).
467 ²⁹ F. Cheynis, F. Leroy, A. Ranguis, B. Detaillieur, P. Bindzi,
468 C. Veit, W. Bon and P. Müller, Combining low-energy electron
469 microscopy and scanning probe microscopy techniques
470 for surface science: Development of a novel sample-holder
471 Review of Scientific Instruments 85, 043705 (2014).
472 ³⁰ F. Cheynis, S. Curiotto, F. Leroy, and P. Mueller, Spatial
473 inhomogeneity and temporal dynamics of a 2D electron gas
474 in interaction with a 2D adatom gas Scientific Reports 7,
475 10642 (2017).
476 ³¹ H. Okamoto, T. B. Massalski, The Au-Ge (Gold-
477 Germanium) system Bulletin of Alloy Phase Diagrams 5,
478 601 (1984).
479 ³² V. Usov, C. O. Coileain, and I. V. Shvets, Influence of elec-
480 tromigration field on the step bunching process on Si(111)
481 Phys. Rev. B 82, 153301 (2010).
482 ³³ See Supplemental Material at [URL will be inserted by
483 publisher] for the time evolution of Au adatom gas under
484 an electric bias by *in situ* LEEM.
485 ³⁴ Richard L. Schwoebel and Edward J. Shipsey, Step Motion
486 on Crystal Surfaces Journal of Applied Physics 37, 3682
487 (1966).
488 ³⁵ Gert Ehrlich and F. G. Hudda, Atomic View of Sur-
489 face Self-Diffusion: Tungsten on Tungsten The Journal
490 of Chemical Physics 44, 1039 (1966).
491 ³⁶ O. Bondarchuk, W. G. Cullen, M. Degawa, E. D. Williams,
492 T. Bole, and P. J. Rous, Biased surface fluctuations due
493 to current stress Phys. Rev. Lett. 99, 206801 (2007).
494 ³⁷ P. J. Rous, Electromigration wind force at stepped Al
495 surfaces Phys. Rev. B 59, 7719 (1999).
496 ³⁸ M. F. G. Hedouin and P. J. Rous, Relationship between
497 adatom-induced surface resistivity and the wind force for
498 adatom electromigration: A layer Korringa-Kohn-Rostoker
499 study Phys. Rev. B 62, 8473 (2000).
500 ³⁹ Kirk H. Bevan, Hong Guo, Ellen D. Williams, and Zhenyu
501 Zhang, First-principles quantum transport theory of the
502 enhanced wind force driving electromigration on Ag(111)
503 Phys. Rev. B 81, 235416 (2010).
504 ⁴⁰ H. Yasunaga, N.J. Wu, S. Yoda, T. Aida, and K. Sakamoto,
505 Atomic layer control by electromigration on semiconductor
506 surfaces Appl. Surf. Sci. 60, 64 (1992).
507 ⁴¹ M. Degawa, H. Minoda, Y. Tanishiro, and K. Yagi,
508 Direct-current-induced drift direction of silicon adatoms
509 on Si(111)-(1 x 1) surfaces Surf. Sci. 461, L528 (2000).
510 ⁴² A.V. Latyshev, H. Minoda, Y. Tanishiro, and K. Yagi,
511 Adatom effective charge in morphology evolution on
512 Si(111) surface Surf. Sci. 401, 22 (1998).
513 ⁴³ K. Thurmer, D.J. Liu, E.D. Williams, and J.D. Weeks,
514 Onset of step antibanding instability due to surface elec-
515 tromigration Phys. Rev. Lett. 83, 5531 (1999).
516 ⁴⁴ V. Usov, S. Stoyanov, C. OCoileain, O. Toktarbaiuly, and
517 I. V. Shvets, Antiband instability on vicinal Si(111) under
518 the condition of diffusion-limited sublimation Phys. Rev.
519 B 86, 195317 (2012).
520 ⁴⁵ E. E. Rodyakina, S. S. Kosolobov, and A. V. Latyshev,
521 Drift of adatoms on the (111) silicon surface under electro-
522 migration conditions JETP Letters 94, 147 (2011).
523 ⁴⁶ R. S. Becker, B. S. Swartzentruber, J. S. Vickers, and
524 T. Klitsner, Dimer-Adatom-Stacking-Fault (DAS) and
525 non-DAS (111) Semiconductor surfaces - A comparison of
526 Ge(111)-C(2x8) to Si(111)-(2x2), Si(111)-(5x5), Si(111)-
527 (7x7), and Si(111)-(9x9) with scanning tunneling mi-
528 croscopy Phys. Rev. B 39, 1633 (1989).
529 ⁴⁷ I. Razado-Colambo, Jiangping He, H. M. Zhang, G. V.
530 Hansson, and R. I. G. Uhrberg, Electronic structure of
531 Ge(111)c(2x8): STM, angle-resolved photoemission, and
532 theory Phys. Rev. B 79, 205410 (2009).
533 ⁴⁸ L Seehofer and RL Johnson, STM study of gold on Ge(111)
534 Surf. Sci. 318, 21 (1994).
535 ⁴⁹ M. Böhringer, P. Molinàs-Mata, J. Zegenhagen, G. Falken-
536 berg, L. Seehofer, L. Lottermoser, R. L. Johnson, and
537 R. Feidenhans'l, Phys. Rev. B 52, 1948 (1995).
538 ⁵⁰ P. B. Howes, C. Norris, M. S. Finney, E. Vlieg, and R. G.
539 van Silfhout, The phase-diagram of annealed Ge(111)/Ga
540 Phys. Rev. B 48, 1632 (1993).
541 ⁵¹ See Supplemental Material at [URL will be inserted by
542 publisher] for the complete movie of the electromigration
543 of Au-poor islands on Ge(111)-1x1 surface.
544 ⁵² HC Jeong and ED Williams, Steps on surfaces: experiment
545 and theory Surf. Sci. Rep. 34, 171 (1999).
546 ⁵³ See Supplemental Material at [URL will be inserted by
547 publisher] for the complete movie of Au-poor islands elec-
548 tromigrating inside the Au-rich phase.
549 ⁵⁴ Kan Nakatsuji, Yuya Motomura, Ryota Niikura, and Fu-
550 mio Komori, Selective doping in a surface band and atomic
551 structures of the Ge(111) ($\sqrt{3} \times \sqrt{3}$)R30 degrees-Au sur-
552 face J. Phys.: Condens. Matter 25, 045007 (2013).